IRAQI BULLETIN OF GEOLOGY AND MINING (IBGM)\
IRAQ GEOLOGICAL SURVEY (GEOSURV-IRAQ)

*IBGM (**2025**, Vol 21; Issue 2)* *25-43*

NEO-TECTONISM ANALYSIS OF THE LINEAMENT STRUCTURES FOR THE GUMAL VALLEY RIVER BASIN, NORTHERN IRAQ

Mosab N. Al-Bana[1*], Najm A. Al-Karai [1], and Ayyed Hussein Ward[1]

[1] Department of Applied Geology, College of Science, Tikrit University, Tikrit, Iraq.
***** Correspondence: mosabjabber@gmail.com; Mosab Al-Bana; ORCID: 0009-0009-7991-1301

Type of the Paper (Article)
Received: 05/02/2025
Accepted: 14/04/2025
Available online: 27/12/2025

Abstract

Lineament analysis is a valuable approach in geological studies and is considered an important structural indicator used to determine regional tectonic directions and local fracture zones. A Digital Elevation Model (DEM) with a resolution of 12.5 m was used to analyze maps and automatically extract lineaments based on parameters defined by the researcher using the PCI Geomatica software for the Gumal Valley basin in northeastern Iraq, which covers an area of 935.12 km². The basin is situated within two tectonic zones: the High Folded Zone in the north and the Low Folded Zone in the south. This paper aims to identify appropriate methods for analyzing automatically extracting lineaments and utilizing the results in tectonic and structural interpretation. Five geospatial analyses were employed for lineament evaluation: length, number, intersection, orientation, and density analysis. The results showed that the lineaments in the region exhibit four main directional trends: NE – SW, NW – SE, N – S, and a secondary E – W trend. The cumulative length and number of lineaments show a predominant NE – SW orientation, which constitutes 52% of the total lineaments. Most major lineaments and faults are located in proximity to each other, with very high lineament density values observed in the High Folded Zone. Morphotectonic analysis of the lineaments revealed good agreement with the orientation of the main regional and local tectonic stress fields, as well as with the drainage pattern and tectonic framework.

Keywords: Morphotectonics; Geological lineaments; GIS & RS; Lineaments extraction; PCI Geomatica.

1. Introduction

The configuration of the Earth's surface is shaped by the combined effects of internal processes (e.g., tectonic and volcanic activity) and external processes (e.g., erosion and deposition) (Hobbs, 1912; Jordan et. al., 2005; Thannoun et al., 2022). The term "Lineament" was first introduced in the early 20th century by Hobbs (1911), who utilized these features and proposed that they result from structural displacement or zones of weakness in the Earth's crust. Hills (1953, as cited in Latman & Nicolson, 1985) was among the first geologists to recognize

ISSN 1811-4539, EISSN 3005-3714 IBGM: http://ibgm-iq.org/
https://doi.org/10.59150/ibgm2102a02 Academic Scientific Journals: www.iasj.net

lineaments as a universal pattern evident in features such as fractures, faults, and major relief forms. Essentially, lineaments are linear or curvilinear structures whose components are aligned in straight or slightly curved segments (Hung et al., 2005; AL-Daghastani & Ghanem, 2018; Al-Jawadi et al., 2022; Soliman et al., 2025). Geomorphological lineaments often correspond well with underlying tectonic structures, such as faults and fractures (Morelli & Piana, 2006; Pal et al., 2006). Lineaments can be derived from two primary data sources: satellite imagery or Digital Elevation Models (DEM). For this study, a DEM was employed due to its high resolution (12.5 m) and the proven effectiveness of the derived results. In the context of remote sensing, geological lineaments can be detected using several methods, which researchers typically classify into three groups:

a. Manual lineament extraction: This method is employed when the primary objective is to identify specific geological features through visual interpretation (Jordan & Schott, 2005).
b. Semi-automatic lineament extraction is a procedure involving an initial automated detection phase followed by manual interpretation and refinement of the detected lineaments (Lim et al., 2001; Jordan & Schott, 2005).
c. Automatic lineament extraction: Lineaments are extracted entirely through computer software analysis of satellite images or Digital Elevation Models (DEM).

2. Materials and methods

The systematic methodology for extracting and analyzing lineaments is illustrated in Figure 1. The approach for this paper consists of six consecutive stages: (i) The first step involves preprocessing and selecting appropriate illumination for the DEM layer to optimize automatic lineament extraction and subsequent morphotectonic analysis. (ii) The second step defines the algorithm parameters using suitable values based on the image resolution and geographical characteristics of the study area. (iii) The third step applies automatic lineament extraction techniques using the LINE module in PCI Geomatica software. (iv) The fourth step involves calculating spatial morphotectonic indices to evaluate the generated lineament map. This includes analyzing the density and spatial distribution of the lineaments, as represented by their lengths, frequencies, and intersection points. (v) The fifth step focuses on analyzing the directional patterns of the lineaments (e.g., rose diagram generation) to identify the main regional and local structural trends. (vi) The final step involves interpreting the results to evaluate the tectonic setting and structural controls of the area based on the derived lineament patterns and morphotectonic indices.

3. Location of the Study Area

The study area is located in northern Iraq, between the cities of Duhok and Mosul, within the Taurus-Zagros fold-thrust belt. This belt comprises two main tectonic zones: the High Folded Zone and the Low Folded Zone. The study area covers 935.12 km² and is geographically situated between longitudes 43°0′0″E and 43°40′0″E and latitudes 36°30′0″N and 37°0′0″N (Figure 2). The Gumal River originates from the Gara Anticline and crosses Atrush, Sheikha, Ain Sifini, and Maqlub folds. The cachment area of the Gumal Valley river includes Gara and Swara tika folds and the eastern parts of Bekhair and Brifka folds, besides Sheikhan, Ain Sifni, Mahad, and Maqlub folds.

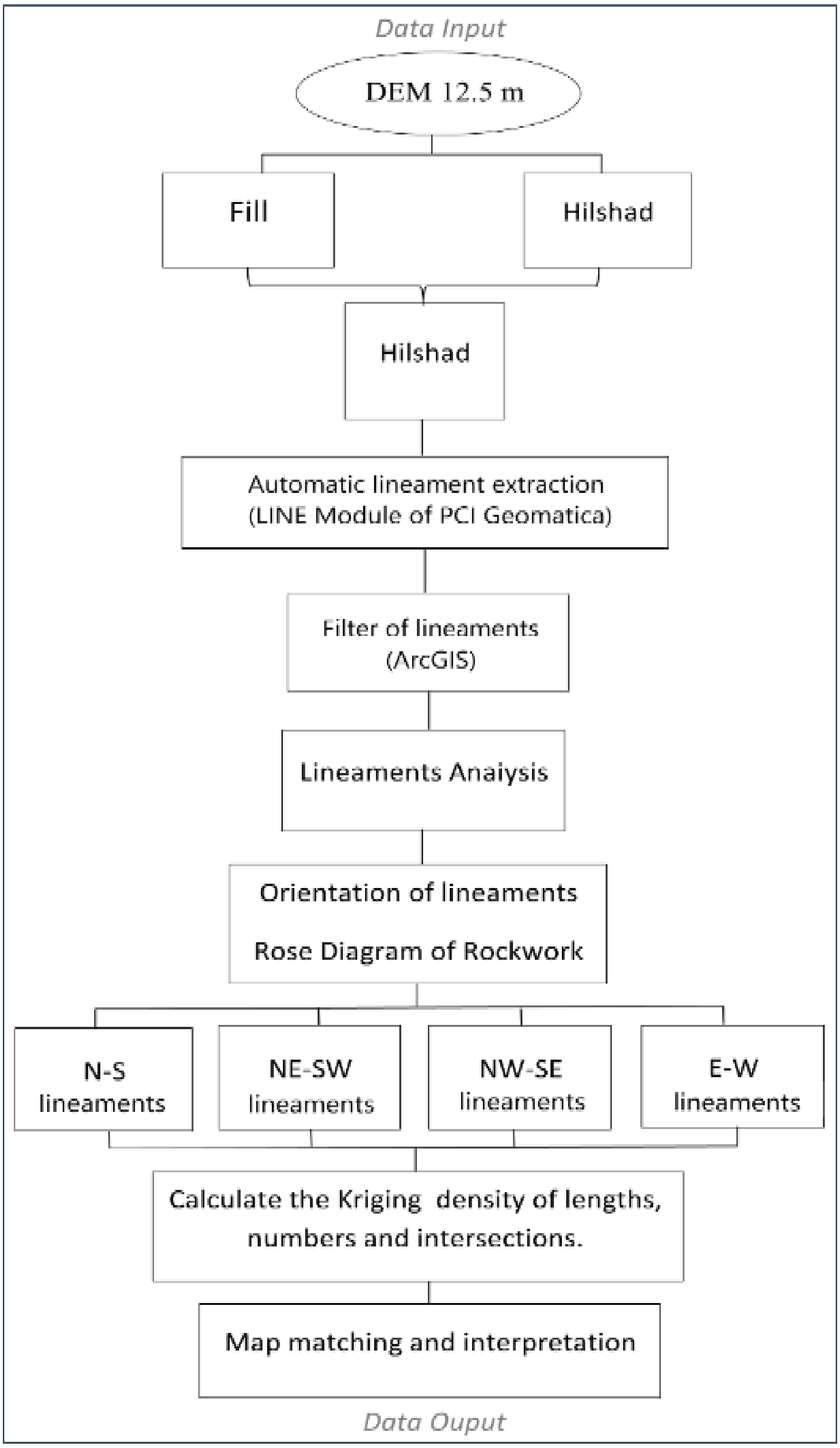

Figure 1. Methodology employed in this research.

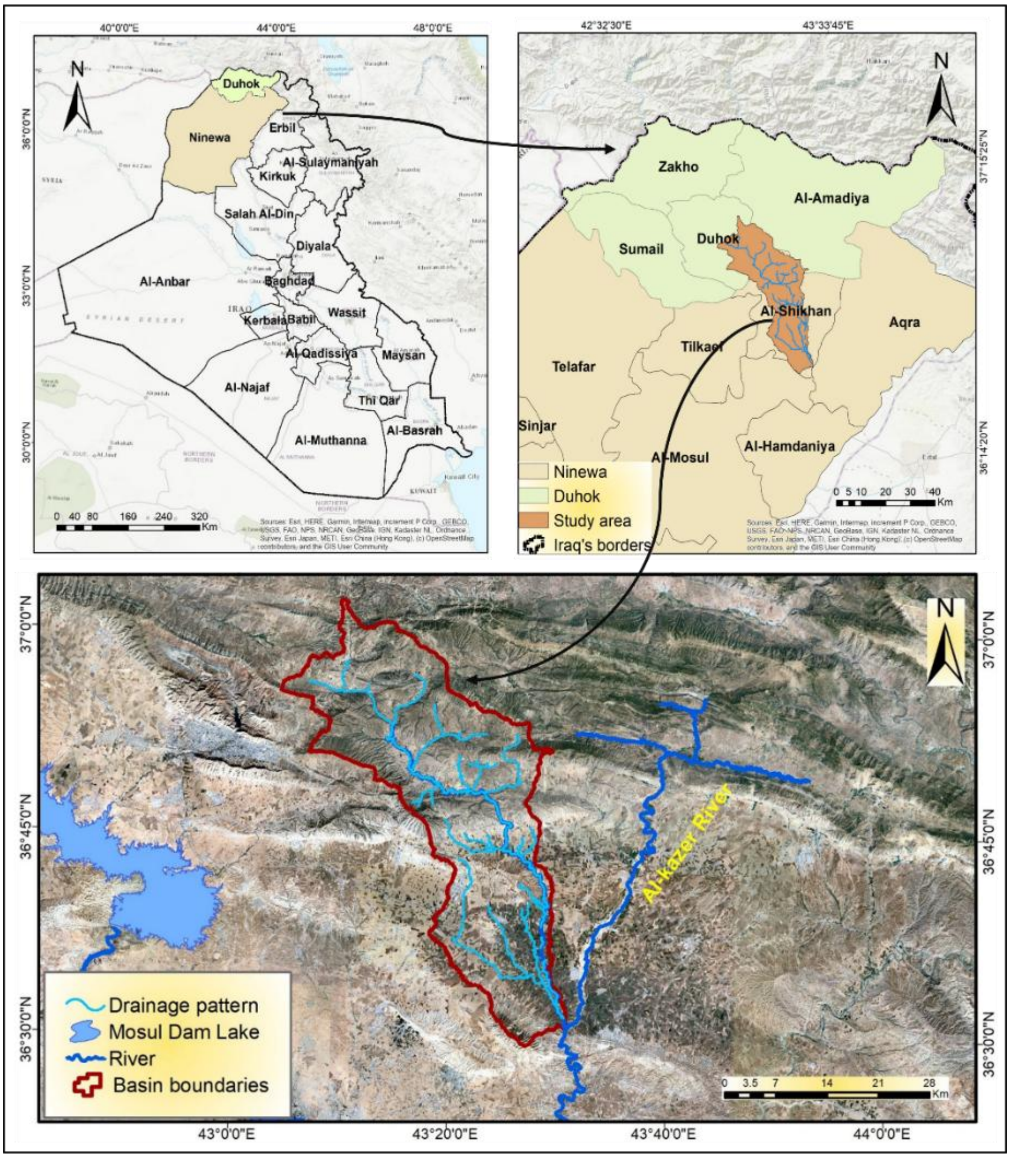

Figure 2. Location of the study area.

4. Geological Setting

4.1. Structural geology

Numerous structural studies (Al-Khatony,2009; Al-Sumaidaie, 2010; Abdullah, 2011; Hamdon & Znad, 2021) have described and analyzed the structural geology of the anticlines in the region. They concluded that fault-related folding originating from these anticlines has directly influenced their vergence and overall configuration, including the alignment of lineament features relevant to this study. Tectonically, the study area represents part of the prominent western Zagros fold-thrust belt, resulting from protracted convergence and collision between the Arabian and Eurasian tectonic plates during the Late Mesozoic and Cenozoic eras (Fu et al., 2024). The tectonics of the Iraqi basement have been affected by inherited basement block faults (with NW – SE and NE – SW trends) extending from the Arabian Shield (Jassim & Goff, 2006). Fold amplification and vergence have been attributed by Numan & Al-Azzawi (1993) to tectonic inversion along listric normal faults dating back to an earlier passive margin phase.

According to Fouad (2015), the study area is located at the boundary between the Low Folded Zone (LFZ) and the High Folded Zone (HFZ; Figure 3). The High Folded Zone occupies the largest portion of the basin, covering an area of 732.67 km², which constitutes 78.35% of the total area (Table 1).

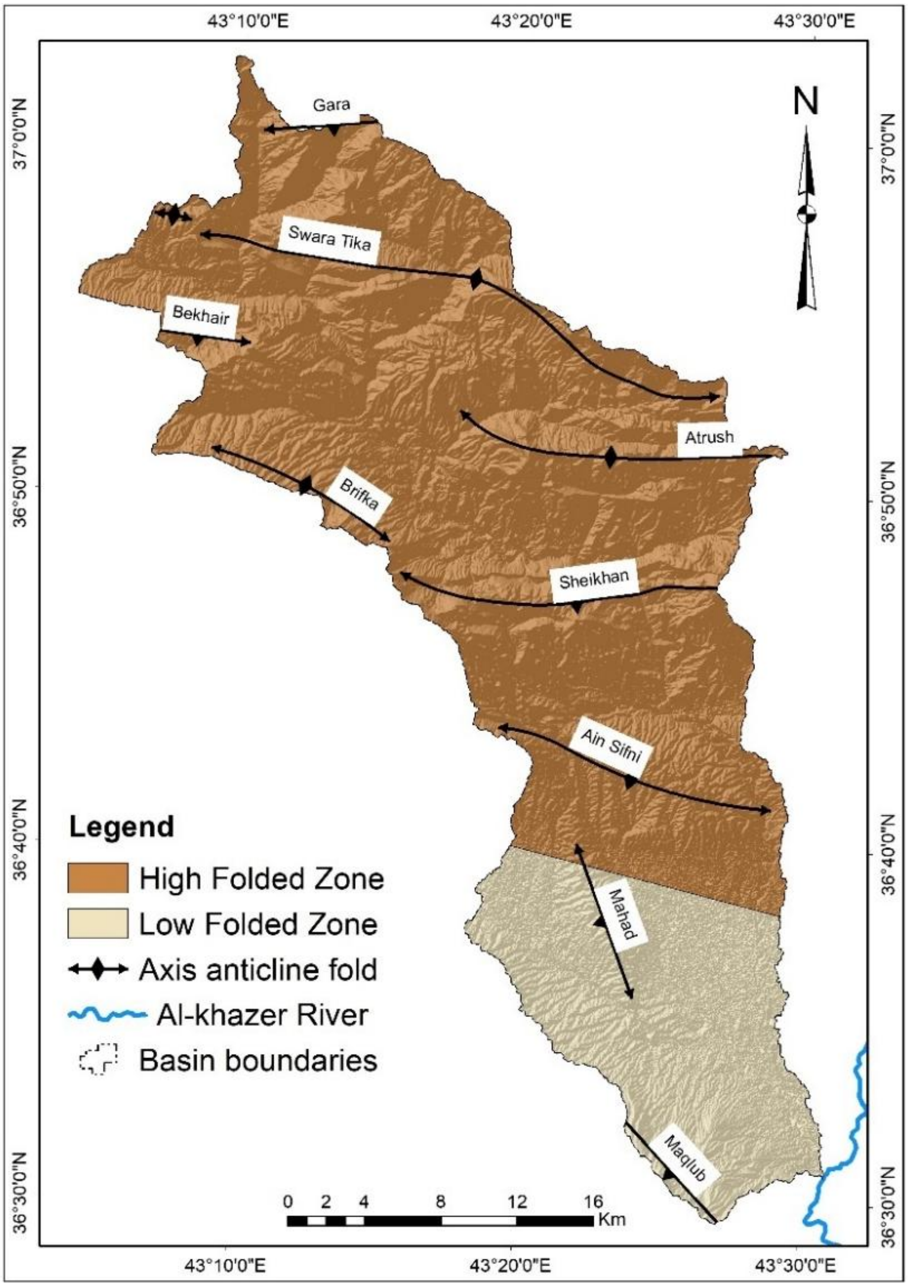

Figure 3. Tectonic division map of the study area (Fouad, 2015).

Table 1. The tectonic, the areas and their percentages.

No.	Tectonic	Area (Km^2)	Percentage (%)
1	High Folded Zone	732.67	78.35
2	Low Folded Zone	202.45	21.64
	Total	935.12	100%

4.2. Stratigraphy

The lithology of geological formations, particularly the contrast in rock competency, is one of the most important natural factors affecting the geometry and distribution of secondary structures such as fractures (including lineaments, faults, joints, and fissures) (Burbank & Anderson, 2001). The study area consists of various formations with hardness ranging from very hard to friable. (Figure 4) presents the geological map, and (Table 2) lists the formations, their ages, and main lithological characteristics, summarised from (Van Bellen & Dunnington, 1959).

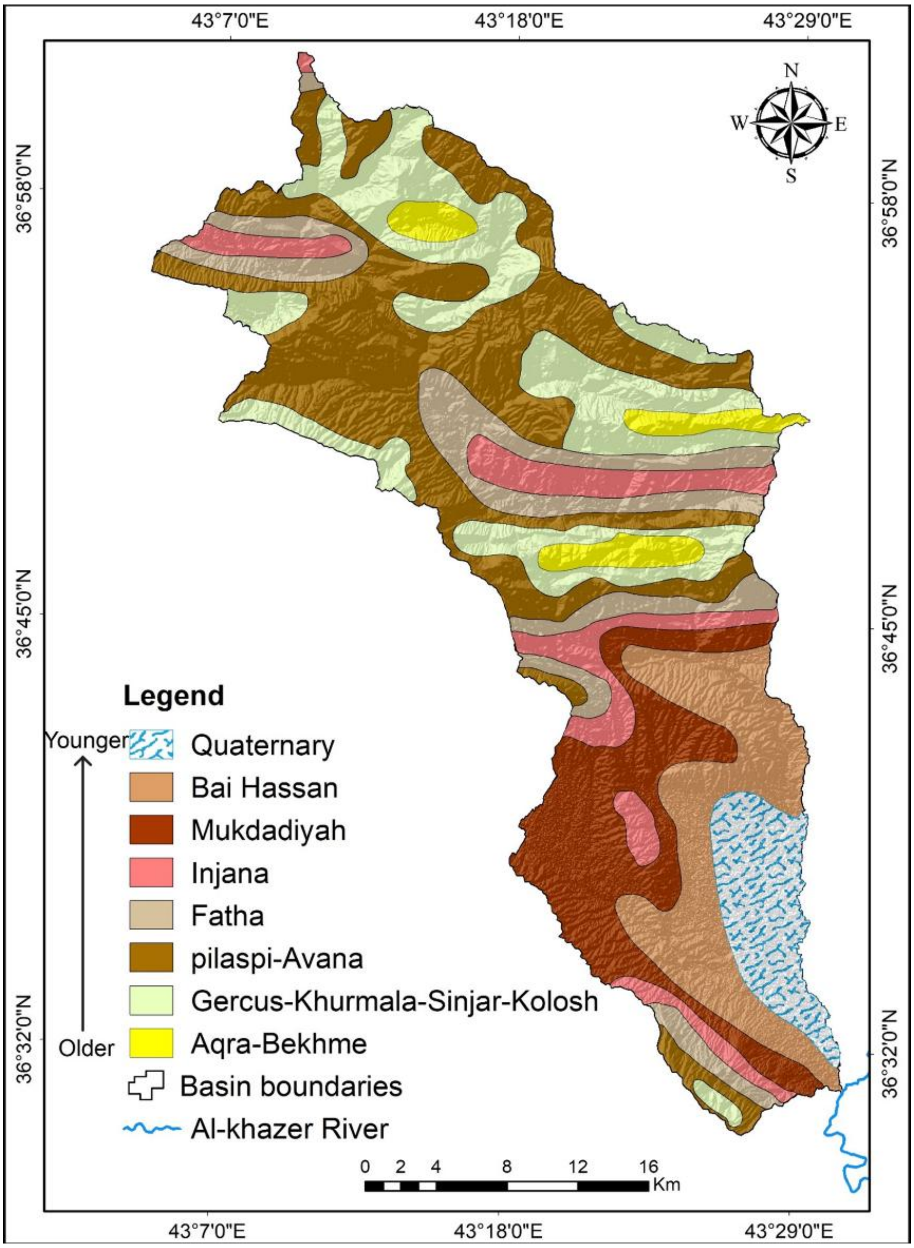

Figure 4. Geological map of the study area (Sissakian & Fouad, 2015).

Table 2. Geological formations of the study area.

No.	Period	Formations	Geological age	Lithology	Area Km^2	%
1	Quaternary	Residual soil	Holocene – Pleistocene	A mixture of sediments consisting of gravel, sand, clay, and silt.	57.24	6.12
2	Neogene	Bai Hassan	Pliocene – Pleistocene.	Conglomerate, sandstone, claystone.	107.53	11.5
3		Mukdadiyah	Late Miocene – Pliocene.	Sandstone, siltstone, claystone.	117.51	12.56
4		Injana	Late Miocene.	sandstone	88.75	9.49
5		Fatha	Middle Miocene.	Limestone, marl, gypsum	103.72	11.09
6	Paleogene	Pilaspi-Avana	Middle – Late Eocene	Limestone	249.1	26.64
7		Gercus, Khurmala, Sinjar, Kolosh	Late Paleocene-Middle Eocene	Claystone, sandstones, conglomerates.	176.55	18.88
8	Cretaceous	Aqra - Bekhme	Campanian-Maastrichtian	Limestones	34.83	3.72
			Total		935.23	100

5. Remote sensing data processing

The automatic extraction parameters, which determine the lengths and numbers of extracted lineaments, depend primarily on the input values set for the LINE module in PCI Geomatica. This module extracts linear features from an image and converts their attributes into vector format using six parameters. The values assigned to each parameter are not fixed; they vary depending on the terrain, area, resolution, and type of image being analyzed. After testing different value combinations for the six parameters, the following values were identified for this case study (Table 3): (RADI; GTHR; LTHR; FTHR; ATHR; DTHR). These parameters are briefly explained by Sarp (2005):

1. Filter radius (RADI): Determines the radius (in pixels) of the edge-detection filter. It approximates the smallest level of detail in the input image to be detected.
2. Gradient Threshold (GTHR): Sets the minimum gradient value for edge pixels to be included in a binary image.
3. Length Threshold (LTHR): Defines the minimum curve length (in pixels) required for a feature to be considered a lineament.
4. Line Fitting Error Threshold (FTHR): Sets the maximum allowable error (in pixels) when fitting a polyline to a pixel curve.

5. Angular Difference Threshold (ATHR): Determines the maximum angle (in degrees) between consecutive polyline segments before a break is created.
6. Linking Distance Threshold (DTHR): Defines the minimum distance (in pixels) between the endpoints of two vectors for them to be linked into one.

Table 3. Parameter values for the LINE Module.

Parameters	Default Values	Suggested Values
Filter Radius	10	8
Edge Gradient Threshold	100	75
Curve Length Threshold	30	20
Line Fitting Error Threshold	3	2
Angular Difference Threshold	30	25
Linking Distance Threshold	20	15

5.1. Results

(Figure 5) shows the map of automatically extracted lineament structures based on the aforementioned parameters in PCI Geomatica. A total of 916 lineaments were extracted, with a cumulative length of 1179.25 km.

Short lineaments typically reflect faults, fissures, and joints in surface rock layers, while longer lineaments and alignments may express subsurface or deep-seated structures and faults in basement rocks resulting from tectonic movements (Al-Karai, 2013). Several authors (Ameen, 1991; Jassim & Goff, 2006) have suggested that the thrust structures in the region result from the reactivation of buried basement faults belonging to the Najd Fault System. In this specific context, the associated forces remain active to the present day (Al-Azzawi, 2003).

5.2. Geometrical Determination of the Orientation Angle

A script in ArcGIS was applied to convert the digitized curved lineaments into straight polylines (Figure 6). The number of lineament segments reached 2421 after this splitting process, which was done to determine the direction of these polylines accurately. The lineaments were classified into four directional trends: N – S, NE – SW, NW – SE, and E – W (Figure 7a & b).

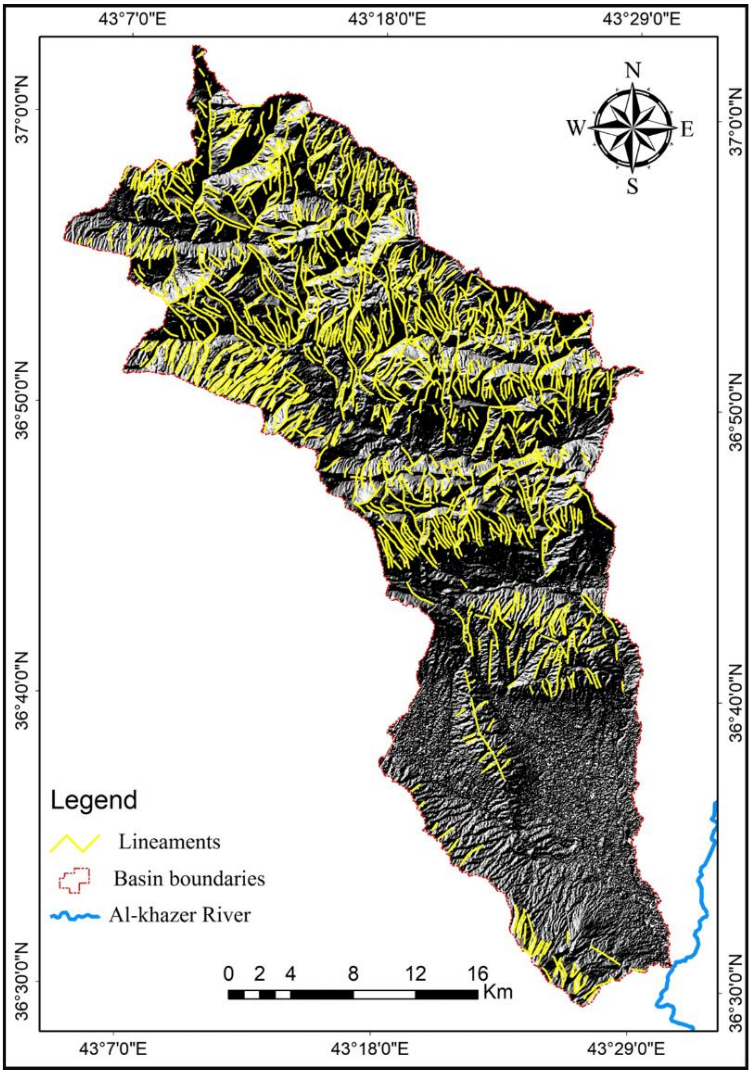

Figure 5. Lineaments obtained through automatic extraction.

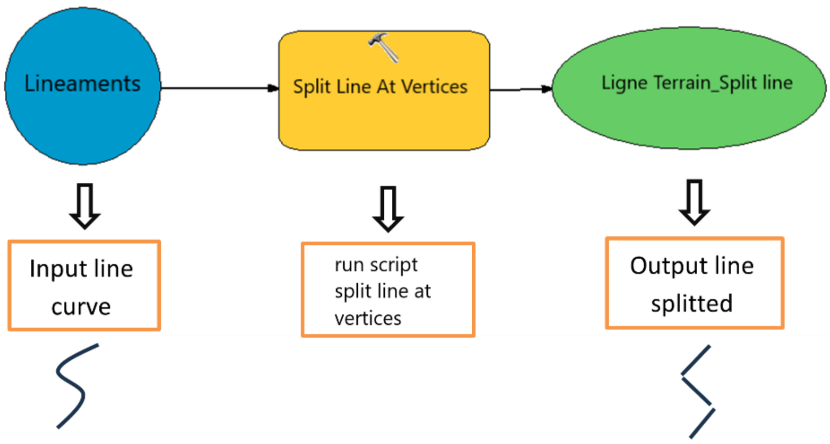

Figure 6. Conversion of digitized lineaments into straight polylines in ArcMap.

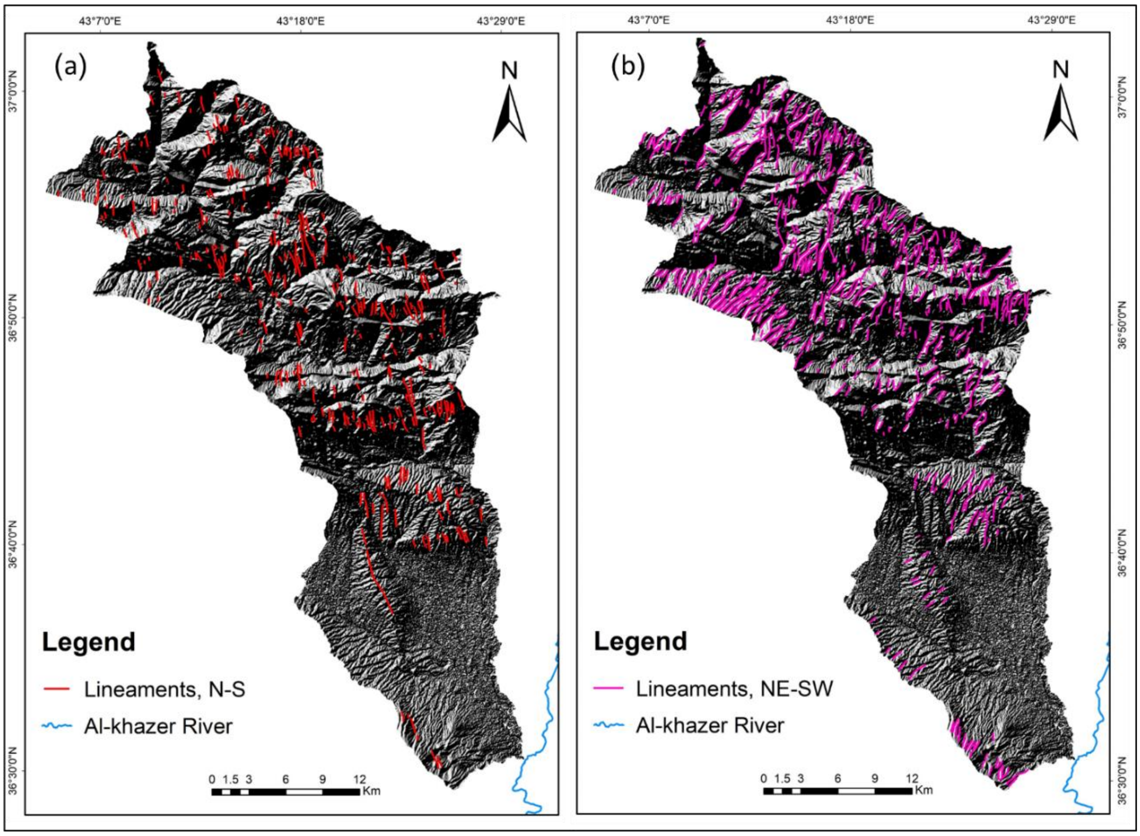

Figure 7a. Lineament map showing two principal trends: **a)** N – S, **b)** NE – SW.

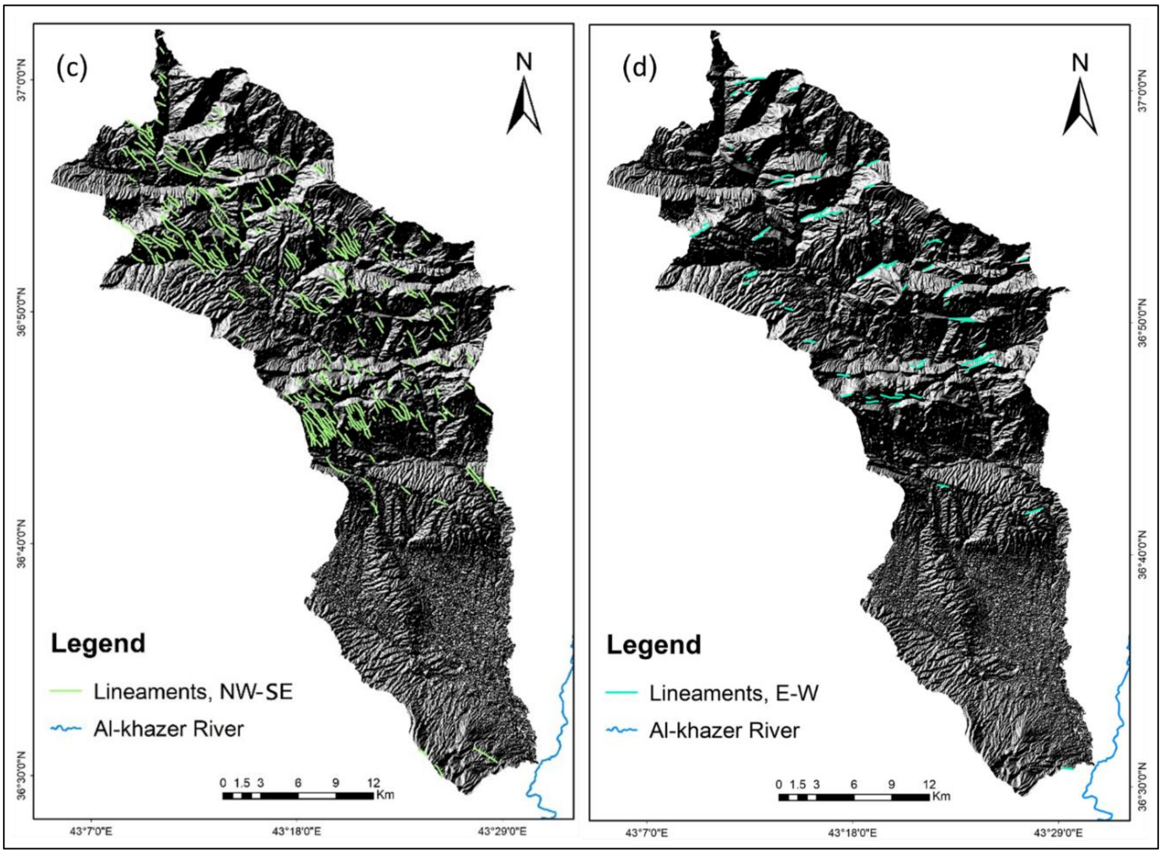

Figure 7b. Lineament map showing two principal trends, **c)** NW – SE, **d**) E – W.

5.3. Calculation of the Start and End Coordinates of Each Lineament

To create a directional rose diagram for all lineaments, the coordinates of each line segment must be calculated. In the lineaments attribute table, the coordinates of the start (X1, Y1) and end (X2, Y2) points were calculated using a script tool in ArcMap. Thus, the lineament directions were categorized (Figure 8). The statistics table was exported to RockWorks16 software to draw rose diagrams for both direction frequency and cumulative length to identify the prevailing trend in the study area (Figure 9). In Table 4, the numbers, lengths, and percentages of lineaments were calculated according to their directions.

As shown in (Figure 7a) and (Table 4), the NE – SW trending lineaments exhibit higher frequency and length compared to other directions. According to the parameter values used in this study, the maximum lineament length (609.53 km) is recorded for the NE – SW direction. Furthermore, the maximum number of lineaments (1237) is also recorded for the same direction. As observed in the rose diagram (Figure 9), the prevailing direction is NE – SW, which also has the greatest cumulative length. This direction accounts for about 52% of the total lineaments.

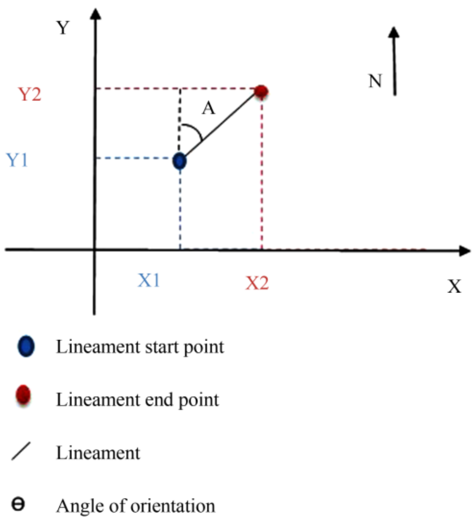

Figure 8. Principle for calculating the orientation of a lineament (Sedrette & Turki, 2015).

Table 4. Length and number of lineaments per direction.

Direction	Lineaments\Km lengths of	%	Number of Lineaments	%
S – N	238.18	20.19	487	20.11
SW – NE	609.53	52.68	1237	51.09
SE – NW	277.15	23.5	573	23.66
W – E	54.39	4.61	124	5.12
Total	1179.25	100	2421	100

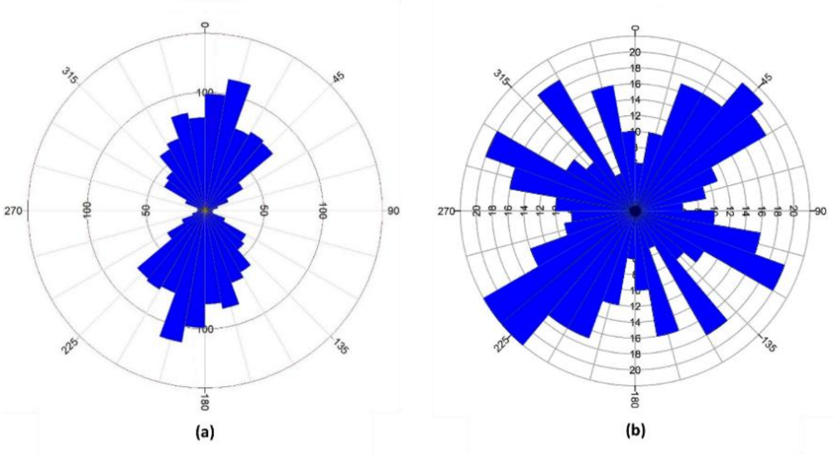

Figure 9. Rose diagram for the lineaments: **a)** direction frequency, **b)** cumulative length.

5.4. Lineaments Density analysis

Following basic statistical analysis, this section examines the linear structures of the Gumal River Valley basin by studying the distribution of their length density, frequency density, and intersection density. The study of linear structure density is linked to several interpretations, including their relationship to tectonic activity for identifying zones of weakness, their influence on landforms, and for mapping the regional extent of faults. On the other hand, these lineament structures play an important role in groundwater exploration, especially at their intersections (Lattman & Parizek, 1964; Magowe & Carr, 1999; Savané & Biémi, 1999; Saley, 2003; Jourda, 2005). Lineaments represent subsurface drainage systems in fractured aquifers (Brunner et al., 2007; Koita, 2017). Relying solely on remote sensing information to identify watersheds is not sufficiently reliable. A combined approach integrating remote sensing and geophysics can address this information gap and significantly reduce uncertainty when implementing water-harvesting structures in bedrock areas (Soro et al., 2017; Akokponhoué, 2019)

This analysis calculates the frequency of lineaments per unit area (Hung et al., 2005) and subsequently creates a map showing lineament intersections per unit area. In this research, length density, frequency density, and intersection density maps were generated using the Spatial Analyst tool in ArcMAP 10.3 by numerically counting lineaments per unit area (number/km², length/km², intersections/km²) and then plotting these values at the center of each corresponding grid cell. The study area was divided into a grid of equal-area squares (5 x 5 km), which were converted to central points to assign the calculated density values. The lengths, numbers, and intersections of the linear structures were measured for each grid cell to calculate the respective densities per km². The total lineament density map (all directions combined) is plotted and presented in (Figuer 10a and b) using both grid cells and contour lines.

A lineament density map is a classification map that depicts the spatial distribution of lineaments within a given area. On these maps, red typically represents the areas with the very highest density of lineaments. The lineaments extracted from the DEM (Figure 10a and b) present the high-density values concentrated mainly in the central parts in HFZ of the map. The maximum density values for lengths, numbers, and intersections reached (177.28, 204.44, and 184.94), respectively. Tables 5, 6, and 7 show the area and percentage of each density.

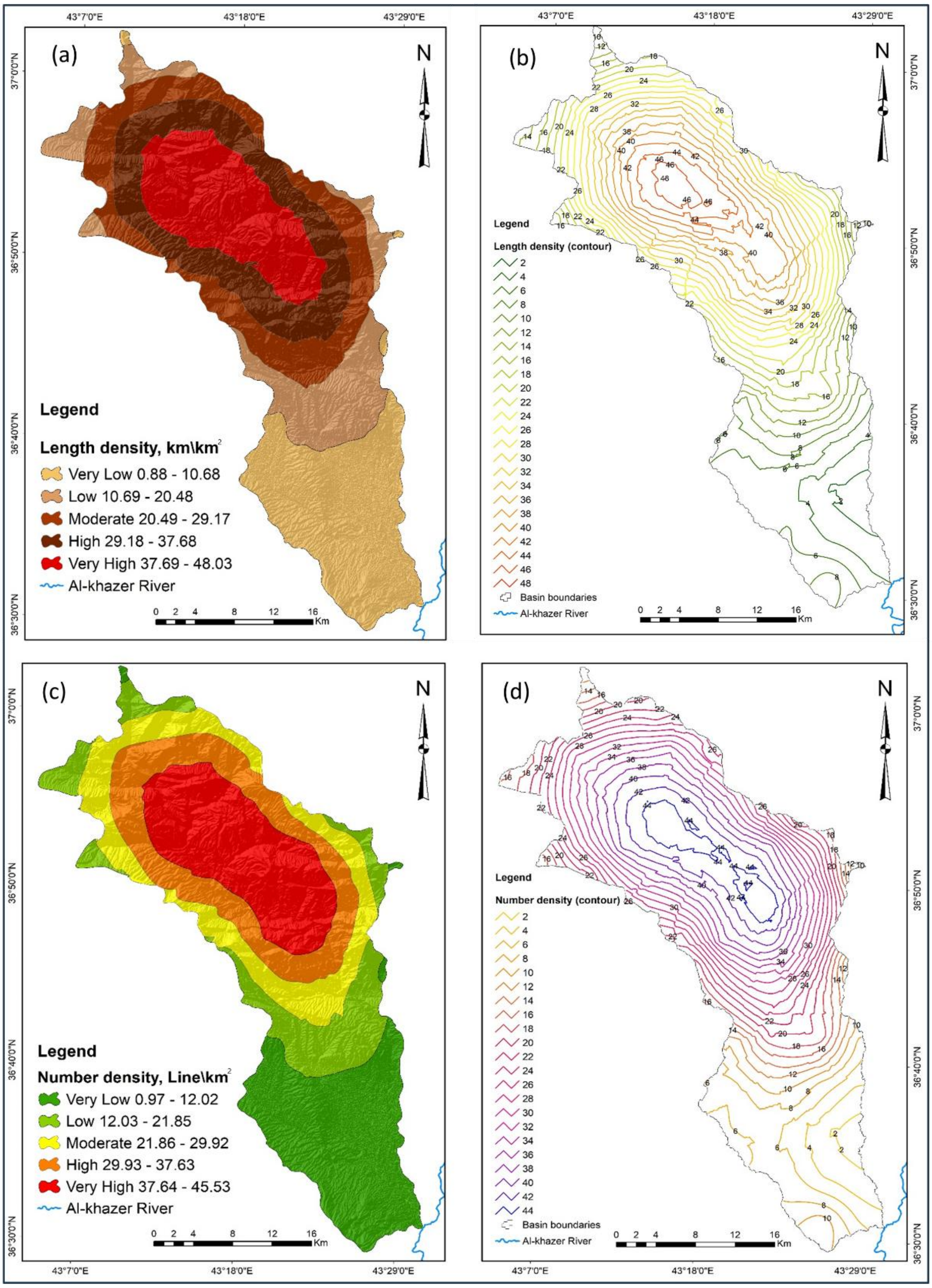

Figure 10a. Lineament density maps by grids and contours. **(a)** and **(c)** grid density for length and number, respectively. **(b)** and **(d)** contour density for length and number, respectively.

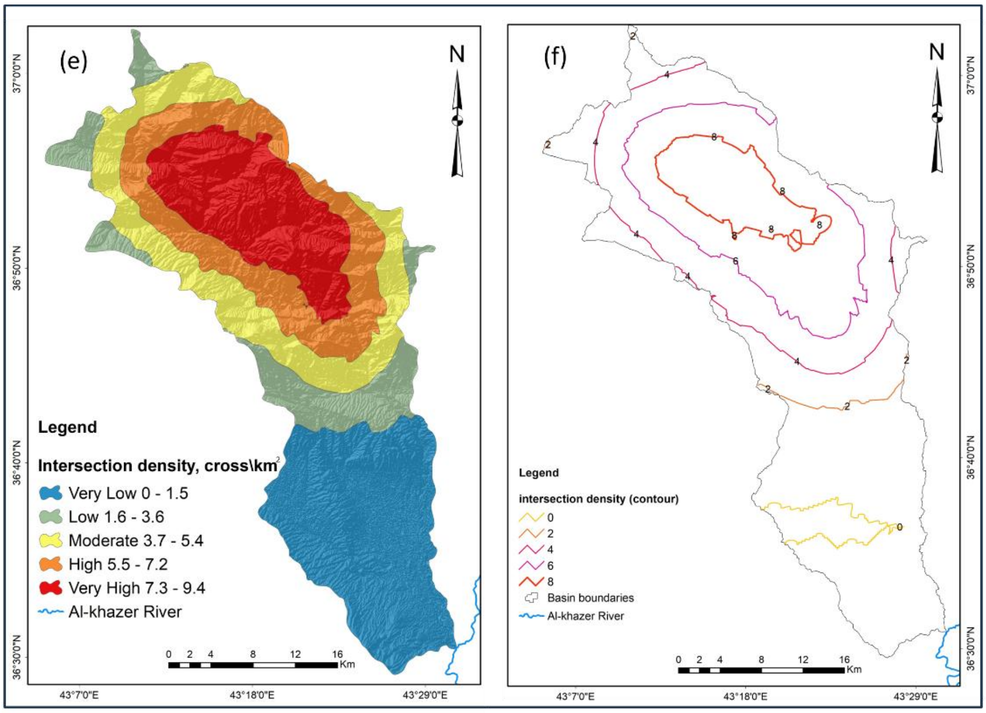

Figure 10b. Lineament density maps by grids and contours. **e)** grid density for intersections, **f)** contour density for intersections.

Table 5. Density of lineament lengths.

Density Class	Density Range (Km\Km^2)	Area	
		km^2	%
Very low	0.88 – 10.68	240.12	25.69
Low	10.69 – 20.48	148.51	15.89
Moderate	20.49 – 29.17	181.31	19.4
High	29.18 – 37.68	187.58	20.07
Very High	37.69 – 48.03	177.28	18.96
Total		100	100

Table 6. Density of lineament numbers.

Density Class	Density Range (Line/km^2)	Area	
		km^2	%
Very low	0.97 – 12.02	239.25	25.59
Low	12.03 – 21.85	139.8	14.95
Moderate	21.86 – 29.92	175.13	18.73
High	29.93 – 37.63	176.27	18.85
Very High	37.64 – 45.53	204.44	21.87
Total		100	100

Table 7. Density of lineament intersections.

Density Class	Density Range (Cross\Km^2)	Area	
		km^2	%
Very low	0 – 15	281.92	30.15
Low	1.6 – 3.6	109.5	11.71
Moderate	3.7 – 5.4	182.27	19.5
High	5.5 – 7.2	176.3	18.86
Very High	7.3 – 9.4	184.94	19.78
Total		100	100

6. Discussion

The detailed automatic analysis of linear features based on the DEM provides insights into the landform structure and geomorphological phenomena of the region, reflecting the influence of tectonic movements. The lineament map derived from this analysis was overlaid with the tectonic map (Figure 11), which serves as a good indicator of neotectonic and morphotectonic processes. This correlation is evident as most lineament directions align with a northeast-southwest trend. This orientation is likely attributed to the collision of the Arabian Plate with the Turkish and Iranian Plates (Mohammad et al., 2014). This collision resulted in the reactivation of strike-slip faults and the development of compressive forces that generated fractures parallel to the main stress direction (NE – SW). The reactivation of these faults creates fractures (lineaments) with a preferred orientation on the Earth's surface.

Therefore, the main compressive stress acts perpendicular to the fold axes. Similarly, the extracted transversal lineaments coincide with the main and local stress directions and are considered indicators of tectonic activity. The stress configuration is displayed in Figure 12. The maximum principal stress axis ($\sigma 1$) aligns with the main N – S directed force, creating dip-slip related joints (Ameen, 1991). The orientations of the shear planes (faults) are consistent with the NE – SW and NW – SE directions, forming conjugate or shear joints. The N – S trending lineaments represent extensional fractures parallel to the major compressive force. The E – W trending lineaments are also considered tensile fractures formed by stress release during the folding process.

The tectonic pattern of the major structural lineaments extracted from the study area can be understood within the tectonic framework of the Taurus-Zagros belt, involving the Anatolian, Eurasian, and Arabian plates. The collision between the Arabian and Eurasian plates during the Eocene (Numan, 1997) resulted in the development of compressive stresses with NE – SW and N – S orientations, depending on the location along the plate boundary. The resulting N – S directed forces show strong coincidence with the extracted lineaments. In this specific setting, the compressive stresses remain effective and influential (Al-Azzawi, 2003).

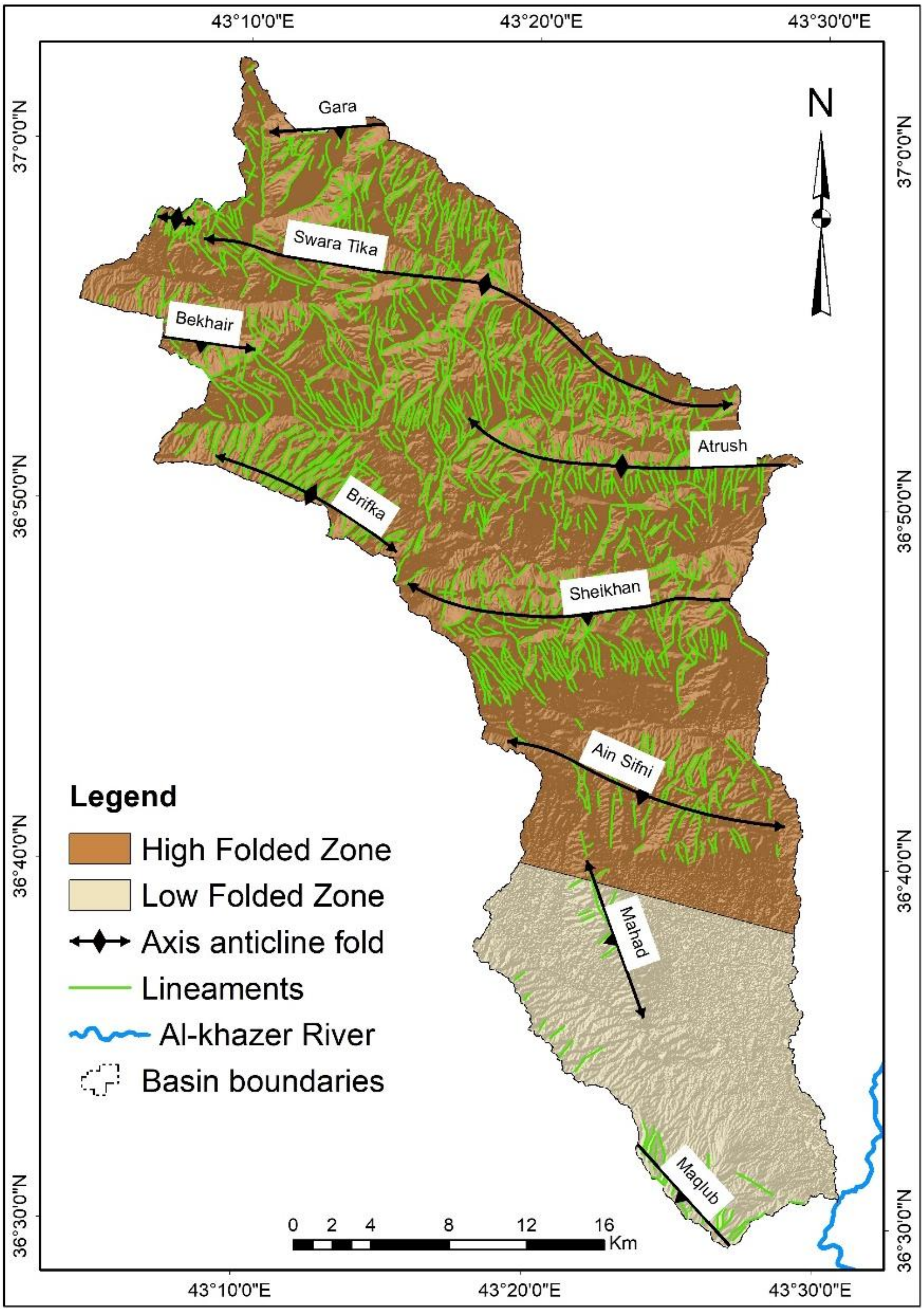

Figure 11. Matching the lineaments map with the tectonic map.

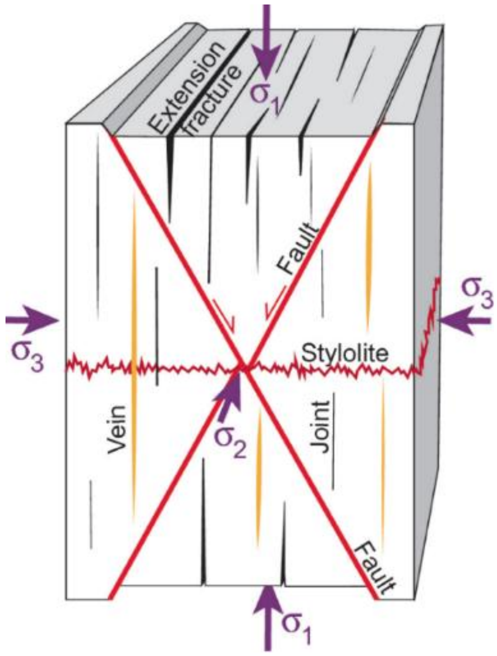

Figure 12. Schematic of the major tectonic stress fields for the research area.

7. Conclusions

- The extracted lineaments reveal all possible linear features that can be represented as fracture zones. The number of lineaments extracted automatically after processing was 2421, most of which are located in the High Folded Zone.
- The NE – SW direction (shear and conjugate joints) is the most common orientation and also has the greatest cumulative length, constituting approximately 52% of the total. This direction is attributed to the collision of the Anatolian Arabian Plate with the Eurasian Plate.
- The lineaments in the NW – SE direction (shear and conjugate joints) rank second in terms of number, constituting 23.66%. They are primarily associated with listric faults, which are parallel to the fold axes corresponding to these lineaments.
- The N – S trending lineaments (Dip joints) represent tension fractures parallel to the major force. In this context, the E – W trending lineaments are also considered tension fractures formed by stress release during folding within the Taurus and Zagros tectonic zones.
- High lineament density (length, frequency, and intersections) is found in areas within the main structural units (High Folded Zone). It is clear that most areas adjacent to major faults also exhibit high lineament density.
- The spatial variation in lineament density is related to lithological and tectonic factors. High-density areas correlate with the presence of brittle Tertiary-Cretaceous carbonate rock formations and proximity to tectonic stress sources, while low-density areas are associated with the more ductile lithologies of Paleogene formations.

References

Abdullah, N. M. R. (2011). *Structural and Tectonic Analysis of the Western Part of Chia Gara Anticline-Northern Iraq*. University of Mosul. (In Arabic)

Akokponhoué, Y. N. , Y. N. , T. M. Y. , A. H. B. , & A. G. (2019). Apport de la télédétection et de la géophysique dans la cartographie des fractures hydrauliquement actives en zone de socle au Centre-Ouest du Benin. *Eur. Sci. J, 15*, 426–447.

Al-Azzawi, N. Q. (2003). The structural development of folds shape in the foreland belt of Iraq and its tectonic implications. *Unpublished Ph.D Thesis, Mosul University, Iraq*.

AL-Daghastani, H. S., & Ghanem, B. G. (2018). Comparison Between Visual and Digital Interpretation of Lineament Features in Allan Anticline, Northern Iraq. *Iraqi National Journal of Earth Science*, *18*(1), 117.

Al-Jawadi, A. S., Bety, A. K. S., & Ismaeel, O. A. (2022). Lineament analysis by using remote sensing and GIS technique of Sangaw Area, Kurdistan Region, NE Iraq. *The Iraqi Geological Journal*, 152–163.

Al-Khatony S. E. M. (2009). *The Structural Analysis and Tectonic Interpretation of Skaikhan Anticline-Northern Iraq*. University of Mosul. (In Arabic)

Al-Karai, N. A., (2013). *The effects lineaments phenomenon and its geomorphology evidences in Allas fold / north Hamereen*. (In Arabic)

Al-Sumaidaie, M. A.-H. (2010). *A tectonic and structural study of the Prevka anticline in northern Iraq.* University of Mosul.

Ameen, M. S. (1991). Alpine geowarpings in the Zagros-Taurus range: Influence on hydrocarbon generation, migration and accumulation. *Journal of Petroleum Geology*, *14*(4), 417-428.

Brunner, P., Hendricks Franssen, H.-J., Kgotlhang, L., Bauer-Gottwein, P., & Kinzelbach, W. (2007). How can remote sensing contribute in groundwater modeling? *Hydrogeology Journal*, *15*(1), 5–18.

Burbank, D. W., Anderson, R. S. (2001). *Tectonic Geomorphology*. *Blackwell Science Malden*. MA.

Fouad, S. F. A. (2015). Tectonic map of Iraq, scale 1: 1000 000, 2012. *Iraqi Bulletin of Geology and Mining, 11*(1), 1–7.

Fu, X., Feng, Z., Zhang, F., Zhang, Z., Guo, J., Cao, Z., Kor, T., Cheng, M., Yan, J., & Zhou, Y. (2024). Wilson cycles of the Zagros fold and thrust belt: A comprehensive review. *Journal of Asian Earth Sciences*, *262*, 105993.

Hamdon, A. N., & Znad, R. K. (2021). An emerging fault related fold (Mahad Anticline) and its morphotectonic interpretations in Northern Iraq. *Iraqi Journal of Science*, 1550–1561.

Hobbs, W. H. (1912). *Earth features and their meaning: an introduction to geology for the student and the general reader*. Macmillan.

Hung, L. Q., Batelaan, O., & De Smedt, F. (2005). Lineament extraction and analysis, comparison of LANDSAT ETM and ASTER imagery. Case study: Suoimuoi tropical karst catchment, Vietnam. *Remote Sensing for Environmental Monitoring, GIS Applications, and Geology V*, *5983*, 182–193.

Jassim, S. Z., & Goff, J. C. (2006). *Geology of Iraq*. DOLIN, sro, distributed by Geological Society of London.

Jordan, G., & Schott, B. (2005). Application of wavelet analysis to the study of spatial pattern of morphotectonic lineaments in digital terrain models. A case study. *Remote Sensing of Environment*, *94*(1), 31–38.

Jordan, G., Meijninger, B. M. L., Van Hinsbergen, D. J. J., Meulenkamp, J. E., & Van Dijk, P. M. (2005). Extraction of morphotectonic features from DEMs: Development and applications for study areas in Hungary and NW Greece. *International journal of applied earth observation and geoinformation*, *7*(3), 163-182.

Jourda, J. P. (2005). Méthodologie d'application des techniques de télédétection et des systèmes d'information géographique à l'étude des aquifères fissurés d'Afrique de l'ouest. Concept de l'Hydrotechnique spatiale: cas des zones tests de la Côte d'Ivoire. *Concept de l'hydrotechnique Spatiale: Cas Des Zones Tests de La Côte d'Ivoire. These de Doctorat d'État, Université de Cocody (Abidjan)*.

Koita, M. (2010). Caractérisation et modélisation du fonctionnement hydrodynamique d'un aquifère fracturé en zone de socle: cas de la région de Dimbokro-Bongouanou (Centre Est de la Côte d'Ivoire) (Doctoral dissertation, Montpellier 2).

Lattman, L. H., & Nickelsen, R. P. (1958). Photogeologic fracture-trace mapping in Appalachian Plateau. *AAPG Bulletin*, *42*(9), 2238-2245.

Lattman, L. H., & Parizek, R. R. (1964). Relationship between fracture traces and the occurrence of ground water in carbonate rocks. *Journal of Hydrology*, *2*(2), 73–91.

Lim, C. S., Ibrahim, K., & Tjia, D. (2001). Radiometric and Geometric information content of Tiung Sat-l MSEIS data. *Tiung SAT-1: From Inception to Inauguration*, 169–184.

Magowe, M., & Carr, J. R. (1999). Relationship between lineaments and ground water occurrence in western Botswana. *Groundwater*, *37*(2), 282–286.

Mohammad, Y. O., Cornell, D. H., Qaradaghi, J. H., & Mohammad, F. O. (2014). Geochemistry and Ar–Ar muscovite ages of the Daraban Leucogranite, Mawat Ophiolite, northeastern Iraq: implications for Arabia–Eurasia continental collision. *Journal of Asian Earth Sciences*, *86*, 151–165.

Morelli, M., & Piana, F. (2006). Comparison between remote sensed lineaments and geological structures in intensively cultivated hills (Monferrato and Langhe domains, NW Italy). *International Journal of Remote Sensing*, *27*(20), 4471–4493.

Numan, N. M. S., and Al-Azzawi, N. K. B. (1993). Structural and geotectonic interpretation of vergence directions of the anticlines in the Foreland Folds of Iraq, Abhath Al-Yarmouk (pure science and engineering), Yarmok University, Jordan, 2, 2, pp. 57- 73.

Numan, N. M. S. (1997). A plate tectonic scenario for the Phanerozoic succession in Iraq. *Iraqi Geological Journal*, *30*(2), 85–110.

Pal, S. K., Majumdar, T. J., & Bhattacharya, A. K. (2006). Extraction of linear and anomalous features using ERS SAR data over Singhbhum Shear Zone, Jharkhand, using fast Fourier transform. *International Journal of Remote Sensing*, *27*(20), 4513–4528.

Saley B. M. (2003). *Système d'informations hydrogéologiques à référence spatiale, discontinuités pseudo-images et cartographies thématiques des ressources en eau de la région sémi- montagneuse de l'Ouest de la Côte d'Ivoire.* Université d'Abidjan.

Sarp, G. (2005). *Lineament Analysis From Satellite Images, North-West Of Ankara*. Middle East Technical University.

Savané, I., & Biémi, J. (1999). Télédétection et SIG pour l'étude des aquifères du socle cristallin d'Odienné (Nord-Ouest de la Côte d'Ivoire). *Télédétection (Amsterdam)*, *1*(1), 47–64.

Sedrette, S. , R. N. and Turki, M. M. (2015). Développement d'une approche quantitative d'extraction semiautomatique des accidents tectoniques de la carte géologique de nefza au 1/50000 en format SHP. *Arabian Journal of Earth Sciences*, 2,53-64.

Sissakian, V. K., & Fouad, S. F. A. (2015). Geological map of Iraq, scale 1: 1000 000, 2012. *Iraqi Bulletin of Geology and Mining*, *11*(1), 9–16.

Soliman, M. A., Yehia, M. A., Omran, A. A., El Sundoly, H. I., Salem, M. M., & Abdelmalik, K. W. (n.d.). *Lithological Discrimination and Lineaments Extraction Using Landsat-8 and Sentinel-2A Data, A Case Study of Gabal Abu Hamr and Gabal Abu Kharif Area, North Eastern Desert, Egypt*.

Soro, D. D., Koïta, M., Biaou, C. A., Outoumbe, E., Vouillamoz, J.-M., Yacouba, H., & Guérin, R. (2017). Geophysical demonstration of the absence of correlation between lineaments and hydrogeologically useful fractures: case study of the Sanon hard rock aquifer (central northern Burkina Faso). *Journal of African Earth Sciences*, *129*, 842–852.

Thannoun, R. G., Adeeb, H. G. M., & Al-Jawadi, A. S. (2022). Extractions morphotectonic features using satellite data processing and DEM-derived spatial models. *The Iraqi Geological Journal*, 88–107.

Van Bellen, R. C., & Dunnington, H. V. (1959). *Lexique stratigraphique international: Asie. Iraq*. Centre national de la recherche scientifique.